# Two-dimensional Bragg grating lasers defined by electron-beam lithography

Guy A. DeRose[a)]
*Department of Electrical Engineering, California Institute of Technology, 1200 E. California Blvd., Pasadena, California 91125 and Department of Applied Physics, California Institute of Technology, 1200 E. California Blvd., Pasadena, California 91125*

Lin Zhu, John M. Choi, and Joyce K. S. Poon
*Department of Electrical Engineering, California Institute of Technology, 1200 E. California Blvd., Pasadena, California 91125*

Amnon Yariv and Axel Scherer
*Department of Electrical Engineering, California Institute of Technology, 1200 E. California Blvd., Pasadena, California 91125 and Department of Applied Physics, California Institute of Technology, 1200 E. California Blvd., Pasadena, California 91125*

(Received 31 May 2006; accepted 2 October 2006; published 30 November 2006)

Two-dimensional Bragg grating (2DBG) lasers with two quarter-wave slip line defects have been designed and fabricated by electron-beam lithography and reactive ion etching. Unlike conventional two-dimensional photonic crystal defect lasers, which use a large refractive index perturbation to confine light in a plane, the 2DBG structures described here selectively control the longitudinal and transverse wave vector components using a weak index perturbation. Two line defects perpendicular to each other are introduced in the 2DBG to define the optical resonance condition in the longitudinal and transverse directions. In this article, we describe the lithography process used to pattern these devices. The 2DBG lasers were defined using polymethylmethacrylate resist exposed in a Leica Microsystems EBPG 5000+ electron-beam writer at 100 kV. A proximity correction code was used to obtain a uniform pattern distribution over a large area, and a dosage matrix was used to optimize the laser design parameters. Measurements of electrically pumped 2DBG lasers showed modal selection in both the longitudinal and transverse directions due to proper design of the grating and defects, making them promising candidates for single-mode, high power, high efficiency, large-area lasers. © *2006 American Vacuum Society.* [DOI: 10.1116/1.2375080]

## I. INTRODUCTION

A major challenge in the fabrication of nanoscale optical structures for the efficient confinement of light in III-V compound semiconductor materials is the need for highly accurate electron-beam lithography and dry etching techniques. Accurate lithography and etching are especially important in the fabrication of the recently proposed two-dimensional Bragg grating (2DBG) lasers.[1–4] Unlike conventional two-dimensional photonic crystal defect lasers,[5,6] which are typically surface emitting and use a large refractive index perturbation to confine light in a plane, the 2DBG structures are edge emitting and selectively control the longitudinal and transverse wave vector components with a weak index perturbation as shown in Fig. 1. Thus, a single laser device has a relatively large area of about $0.8 \times 0.16$ mm$^2$ consisting of about a quarter of a million small holes each with a radius of only 100 nm. The large difference in scale between the device area and the grating feature size (i.e., the hole area), nearly seven orders of magnitude, presents a fundamental challenge to the fabrication process.

2DBG lasers require highly uniform patterns defined by electron-beam lithography over a large area, such that the holes for a single device should be nearly identical. A nonuniform index perturbation in our structures that can be caused by the size variation of small holes results in undesired chirp or variation in the grating period leading to spectral broadening in the gratings. To achieve the uniformity required in 2DBG lasers, proximity effect correction in the electron-beam lithography is required.

Proximity effect refers to the dependence of the actual electron-beam exposure dosage on the density of local features, and it has been the major problem for obtaining fine resolution and large-area uniformity in electron-beam lithography. Electrons incident on a resist layer experience forward and backward scatterings in the resist. In addition to exposing the desired areas, the scattered electrons can also expose the areas beyond the designed patterns. A Monte Carlo simulation of this scattering of 100 keV electrons in the material stack used in this article is shown in Fig. 2 and illustrates that the scattered electrons can expose the polymethylmethacrylate (PMMA) "from below" laterally outside of the beam spot. The relevant length scale to determine the significance of the proximity effect is given by the backscattering length $\beta$, and this parameter is calculated numerically for the material system by the Monte Carlo simulation program. This deleterious scattering has a slight impact on isolated patterns, such as the holes near the edges of our structure. However,

a)Author to whom correspondence should be addressed; electronic mail: derose@caltech.edu

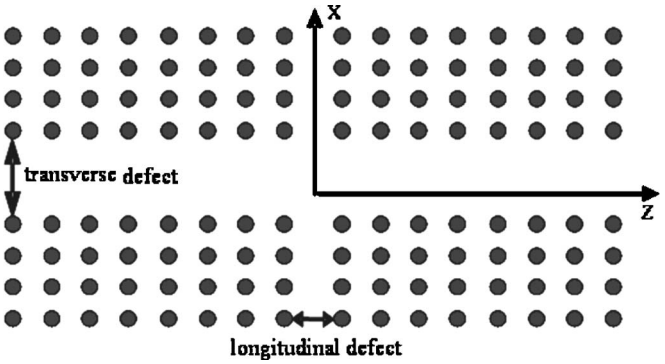


FIG. 1. Illustration of the two-dimensional Bragg grating laser (2DBG) with two line defects. The laser output is taken along the $z$ direction.

for dense patterns, such as the holes in the center region of our structure, this undesired exposure can be significant. Therefore, if a constant electron dosage is used over the pattern area, the actual, effective exposure dosage of the holes around the center will differ from that at the edge, manifesting in pattern distortion due to the proximity effect.

In this article, we describe the fabrication process of 2DBG lasers and discuss the effect of proximity effect correction. The 2DBG lasers were defined using PMMA resist exposed in a Leica Microsystems EBPG 5000+ electron-beam writer at 100 kV. To correct for the proximity effect, we use commercially available software, described in Sec. III. We found that the uniformity of the pattern distribution improved by the use of proximity correction as a function the aggressiveness of the correction. Measurements of electrically pumped 2DBG lasers showed modal selection in both the longitudinal and transverse directions due to the proper design of the grating and defects. Our demonstration illustrates that 2DBG lasers are promising candidates for single-mode, large-area lasers for high power applications.

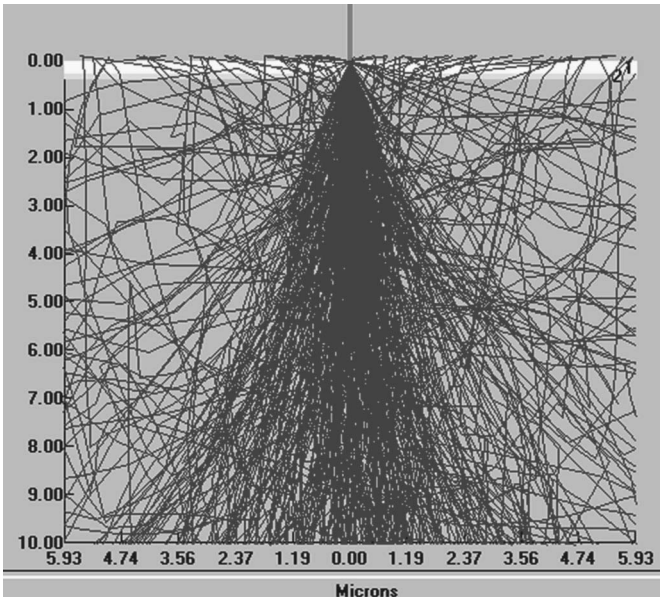


FIG. 2. Monte Carlo simulation of 100 keV electrons scattering in the material stack. The top (white) layer is 250 nm PMMA. The second layer (light gray) is 120 nm $SiO_2$, and the substrate (dark gray) is InP. The ordinate is the radial distance in $\mu$m from the incident beam spot and the abscissa is penetration depth in $\mu$m into the material.

## II. FABRICATION

We fabricated 2DBG lasers in commercially grown active semiconductor materials. The semiconductor material had InGaAsP layers totaling a thickness of 725 nm on top of an InP substrate. Four 75-Å-wide unstrained InGaAsP quantum wells and their barrier layers are located at 675 nm from the top wafer surface (8.5 nm wells; 10 nm barriers, $\lambda_g = 1.2$ $\mu$m). The peak photoluminescence from quantum wells was around 1548 nm. A 120-nm-thick $SiO_2$ layer was first deposited by plasma enhanced chemical vapor deposition on the top of the wafer. Then, a 250 nm 495K C4 PMMA (Microchem) resist layer was spun on the substrate at 4000 rpm and baked at 180 °C for 3 min. We exposed the PMMA resist in a Leica Microsystems EBPG 5000+ direct electron-beam writer at an accelerating voltage of 100 kV and a beam current of 3.9 nA. Development of the patterned PMMA film was carried out in a solution of 1:3 methyl-isobutyl ketone:isopropanol for 60 s.

After development, the PMMA patterns were transferred to the $SiO_2$ layer by reactive ion etching (RIE) using $CHF_3$ plasma, with a $CHF_3$ flow rate of 20 SCCM (SCCM denotes cubic centimeter per minute at STP), chamber pressure of 60 mTorr, and rf power of 110 W. The plasma dc self-bias was about 455 V, and the etch rate was around 40 nm/min. The $SiO_2$ layer then served as a hard mask to etch the semiconductor surface grating using an inductively coupled plasma (ICP)-RIE with HI/Ar chemistry.[7] In the etch recipe used, the HI/Ar gas flow was 10/6 SCCM, the chamber pressure was 5 mTorr, and the ICP and rf electrodes were driven with 650 and 30 W, respectively. The plasma dc self-bias was around 104 V, and the etch rate was about 250 nm/min. After the ICP-RIE etch, the remaining $SiO_2$ was stripped off in a buffered hydrofluoric acid solution.

Next, we deposited the top electrical ($p$-type) contacts onto the devices via lift-off. A 1.8 $\mu$m thick layer of Shipley 1813 photoresist layer was used for the lift-off. The $p$-type electrical contacts, Cr/AuZn/Au, were thermally evaporated on the device surface. The lift-off was carried out in acetone solution in an ultrasonic bath for 1 min. The chip was then mechanically lapped down to around 100 $\mu$m. The $n$-type contacts, Cr/AuGe/Au, were then evaporated onto the devices. Finally, we cleaved the devices off the chip.

## III. PROXIMITY EFFECT CORRECTION

An important step toward achieving the uniformity required in 2DBG lasers is highly accurate electron-beam lithography to transfer the pattern to the resist. To this end, proximity effect correction is critical. To characterize the extent of the proximity effect and to determine the degree of proximity effect correction required, we quantitatively compare the feature sizes at various regions of the pattern with various degrees of correction. Our test pattern consists of a $96 \times 96$ $\mu m^2$ square array of holes with a designed radius of

100 nm spaced at a period of 480 nm. The size of the test pattern was sufficient in modeling the lithography of the actual 2DBG lasers which consisted of a square array of holes of the same radius and period but over a much larger area of $\sim 800 \times 160\ \mu m^2$.

The calculations to determine the dose variations required to compensate for the proximity effect fall into three stages. The first stage is a Monte Carlo simulation of the scattering of the incident electron beam as it passes through the various layers of the material "stack." We used a commercial numerical simulation package for this calculation called SCELETON (scattering of electrons in matter) by PDF Solutions aiss division (licensed by Synopsys, Inc. to work with PROXECCO and CATS). This program takes a user-defined resist-substrate multilayer stack of components defined in a materials database and traces a specified number of electrons in the material. Monte Carlo simulation is carried out using a single scattering model, where the electron trajectory is followed through a series of scattering events in the resist/substrate stack. Elastic scattering events are described using the screened Rutherford formula. The backscattering range $\beta$ is determined numerically and applied to the material system by calculation of the proximity function,

$$f(r) = \frac{1}{\pi(1+\eta)}\left(\frac{1}{\alpha^2}\exp(-r^2/\alpha^2) + \frac{\eta}{\beta^2}\exp(-r^2/\beta^2)\right),$$

where $\alpha$ is the width of the direct exposure, $\beta$ is the width of backscattering, and $\eta$ is the ratio between the exposure coming from the direct and that from the backscattered electrons.[8]

Energy dissipation due to inelastic scattering is modeled by Bethe's energy loss formula in the continuously slowing down approximation. Typical calculation time for the stack used in this article was 11 h on a LINUX-based Xeon processor system in which $1 \times 10^7$ electrons were traced. The resulting calculated radial energy density distribution (point spread) can be used directly as input for PROXECCO.

The Monte Carlo simulation results are used as input for the program PARAPROX, which determined what is called the proximity function. The mathematical algorithm of PROXECCO uses a fast variant of the deconvolution method which describes the physics behind the proximity effect very well. The accuracy and efficiency is based on a separate treatment of pattern and correction. PROXECCO performs a determination of this proximity function in a plane of the resist specified by the user and then calculates the correction factors, or conditional frequency assignments (CFAs), to apply when fracturing the pattern data. A particularly useful feature of this approach is that it treats the material stack and pattern data independently, which vastly improves both the flexibility of application and speed of computation.

The CFA data file is used by the fracturing program (CATS by Transcription Enterprises, now licensed by Synopsys, Inc.) by convolution with the proximity parameter file to prepare the pattern data for exposure with variable doses such that the effective dose over the pattern is uniform. The number of conditional frequency assignments determines how fine the variation of the dose is. The number of CFAs to use is something to be determined experimentally, as too few factors result in undercorrection and too many factors result in excess computational and exposure time.

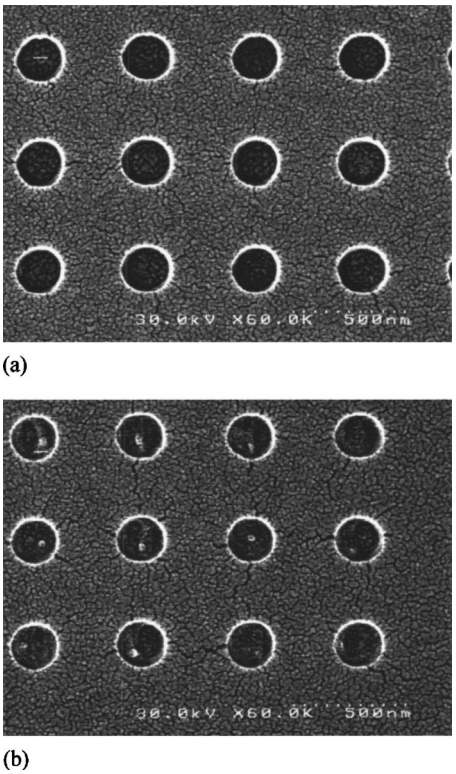


FIG. 3. Scanning electron micrographs of the PMMA resist after uncorrected electron-beam lithography at a dosage of 700 $\mu C/cm^2$. At this dosage, the radius of the holes in the center region is closest to the designed value. (a) The holes at the center of the test pattern. (b) The holes at the edge of the test pattern.

### A. Without proximity effect correction

We first characterized the electron-beam lithography without any proximity effect correction. We found that at an electron-beam dosage of 700 $\mu C/cm^2$, while the radius of the holes in the central region was closest to the designed value, the holes at the edge of the pattern were underexposed as shown in Fig. 3. However, when the holes near the edge were sufficiently exposed and closest to the designed size, the central region was overexposed.

Figure 4 shows the relative error in the hole sizes as a function of the distance from the center of the pattern when the holes at the edges had the minimum size error and sufficient dosage such that no PMMA remained. The relative error (RE) is defined as

$$\mathrm{RE} = \frac{r_d - r_c}{r_c},$$

where $r_c$ is the measured hole radius at the center of the pattern and $r_d$ is the measured hole radius at a particular distance from the center. RE represents the uniformity for the whole pattern. The solid line in Fig. 4 shows the RE for the

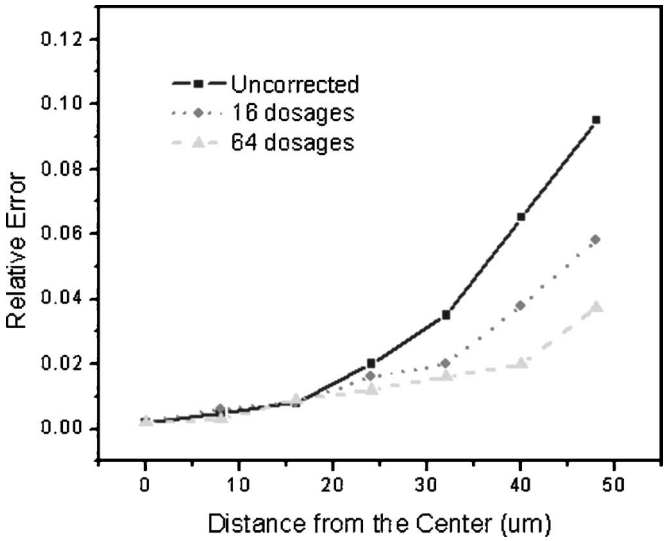


FIG. 4. Relative error in the hole radius as a function of the distance from the center of the pattern for different degrees of proximity effect correction. The solid line is for the uncorrected lithography with a dosage of 750 $\mu$C/cm$^2$. The dotted line is for the corrected lithography using a set of 16 dosages centered at 260 $\mu$C/cm$^2$. The dashed line is for the corrected lithography using a set of 64 dosages centered at 230 $\mu$C/cm$^2$.

lithography without proximity effect correction for a dosage of 750 $\mu$C/cm$^2$. The sizes of the holes varied up to 10% over the test pattern area. This variation would be sufficient to result in chirped gratings that would modify the spectral properties of the 2DBG lasers.

### B. With proximity effect correction

To compensate for the proximity effect, we used CATS with proximity correction, as described above, which fractures the pattern into a large number of divisions and assigns one of the set of defined dosages to each division. The required dosage is calculated by the program from the pattern density while accounting for the resist and substrate electron scattering properties. We repeated the electron-beam lithography with sets of 16 and 64 dosages in the proximity effect correction program.

The dashed and dotted lines in Fig. 4 show the relative hole size errors for the two cases. Again, the relative error is taken at the dosage range where the holes near the edges of pattern are exposed and of minimum relative error. As shown in Fig. 4, a set of 16 dosages resulted in a maximum relative size error of 6% at the edge region of the pattern. Sixty-four dosages were required to limit the error to less than 4%, which is acceptable for our 2DBG laser designs. Therefore, for the fabrication of the 2DBG lasers, we used 64 dosages in the proximity effect correction code to obtain sufficiently uniform gratings over the large area ($\sim 800 \times 200$ $\mu$m$^2$) of the device.

## IV. MEASUREMENT RESULTS

The 64-CFA laser bars were cleaved to lengths of about 1 mm and tested in pulsed operation with no active cooling.

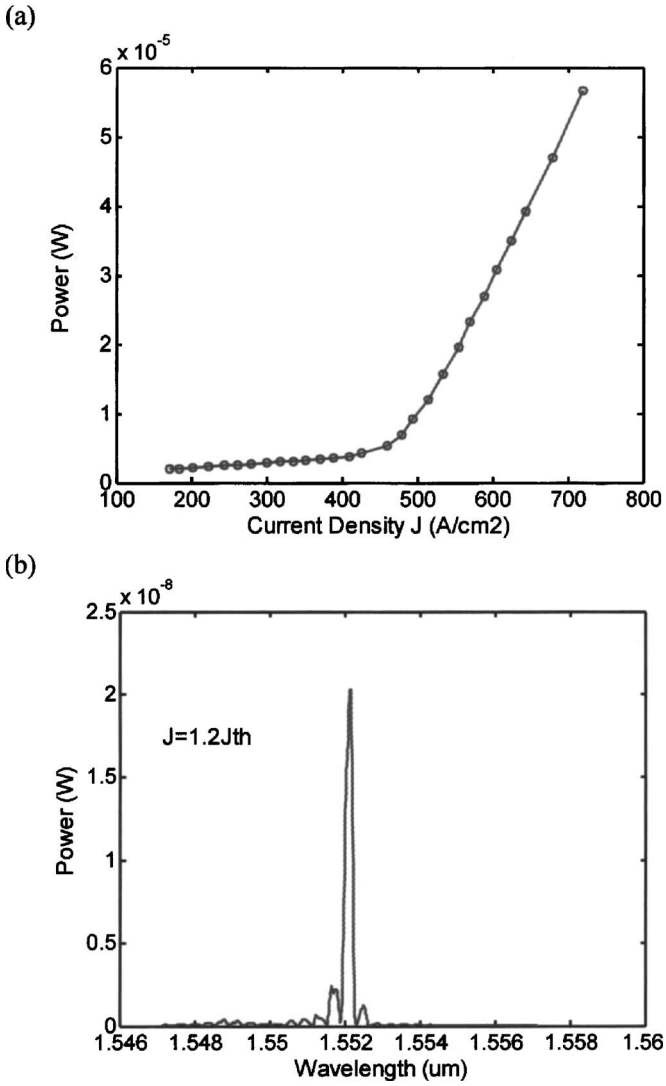


FIG. 5. (a) Light-current density curve with a clear threshold at 442 A/cm$^2$ (average power vs peak current density). (b) Laser spectrum above the threshold at 1.2 times greater than the threshold pump current.

Current pulses with duration of 50 ns and a period of 50 $\mu$s were injected to drive the lasers. The light-current density curve is shown in Fig. 5(a) with a clear threshold occurring at 442 A/cm$^2$, indicating the onset of laser action.

The laser spectrum above the threshold obtained at a pumping current density of $J=1.2J_{\text{th}}$ is illustrated in Fig. 5(b), showing multiple laser modes. The free spectral range (FSR) is about 0.36 nm, corresponding to a length of 1.04 mm ($L=\lambda^2/2n_g\lambda_{\text{FSR}}$,[9] $n_g$ is assumed to be 3.2). The FSR suggests that these emission peaks arose from the longitudinal modes of the laser defined by end facets. Compared to a typical transverse Bragg resonance laser spectrum in Ref. 4, which is similar to a broad area laser spectrum, the spectrum in Fig. 5(b) shows that the grating in the fabricated 2DBG laser can control the longitudinal modes. Since we did not apply antireflection coatings at the end facets, some longitudinal modes due to the Fabry-Pérot resonances from the facet reflection still remained around the main laser peak.

## V. CONCLUSION

In summary, we have fabricated and measured two-dimensional Bragg grating lasers in InP/InGaAsP. Due to the large difference in scale between the grating feature size and the device size, coupled with the contribution of the range of backscattered electrons, proximity effect correction in the electron-beam lithography was paramount in obtaining an accurate pattern. Our demonstration of the improved modal control afforded by the two-dimensional Bragg gratings illustrates the feasibility of large-area, single-mode lasers.

## ACKNOWLEDGMENT

The authors would like to acknowledge funding by DARPA under Contract No. HR0011-04-1-0032.

[1]L. Zhu, J. M. Choi, G. A. DeRose, A. Yariv, and A. Scherer, Opt. Lett. **31**, 1863 (2006).
[2]A. Yariv, Opt. Lett. **27**, 936 (2002).
[3]A. Yariv, Y. Xu, and S. Mookherjea, Opt. Lett. **28**, 176 (2003).
[4]J. M. Choi, L. Zhu, W. Green, G. DeRose, and A. Yariv, 24th International Congress on Applications of Lasers and Electro-optics, ICALEO 2005 (unpublished), Paper No. 406.
[5]M. Loncar, T. Yoshie, A. Scherer, P. Gogna, and Y. Qiu, Appl. Phys. Lett. **81**, 2680 (2002).
[6]H. G. Park, S. H. Kim, S. H. Kwon, Y. G. Ju, J. K. Yang, J. H. Baek, S. B. Kim, and Y. H. Lee, Science **305**, 1444 (2004).
[7]W. Green, J. Scheuer, G. DeRose, and A. Yariv, Appl. Phys. Lett. **85**, 3669 (2004).
[8]H. Eisenmann, T. Waas, and H. Hartmann, J. Vac. Sci. Technol. B **11**, 2741 (1993).
[9]A. Yariv and P. Yeh, *Photonics: Optical Electronics in Modern Communications*, 6th edition (Oxford University Press, New York, 2007), p. 163.